Journal of Electronic Imaging 9(2), 170–177 (April 2000).

Counting white blood cells using morphological granulometries

Nipon Theera-Umpon
Department of Electrical Engineering
University of Missouri–Columbia
Columbia, Missouri 65211
E-mail: nipon@ece.missouri.edu

Paul D. Gader
Department of Computer Engineering and Computer Science
University of Missouri–Columbia
Columbia, Missouri 65211
E-mail: gader@ece.missouri.edu

Abstract. *We describe a modification of the mixture proportion estimation algorithm based on the granulometric mixing theorem. The modified algorithm is applied to the problem of counting different types of white blood cells in bone marrow images. In principle, the algorithm can be used to count the proportion of cells in each class without explicitly segmenting and classifying them. The direct application of the original algorithm does not converge well for more than two classes. The modified algorithm uses prior statistics to initially segment the mixed pattern spectrum and then applies the one-primitive estimation algorithm to each initial component. Applying the algorithm to one class at a time results in better convergence. The counts produced by the modified algorithm on six classes of cells—myeloblast, promyelocyte, myelocyte, metamyelocyte, band, and PolyMorphoNuclear (PMN)—are very close to the human expert's numbers; the deviation of the algorithm counts is similar to the deviation of counts produced by human experts. The important technical contributions are that the modified algorithm uses prior statistics for each shape class in place of prior knowledge of the total number of objects in an image, and it allows for more than one primitive from each class.* © *2000 SPIE and IS&T.*
[S1017-9909(00)00602-4]

1 Introduction

Estimates of the relative numbers of different types of white blood cells in bone marrow aid in the diagnosis of diseases such as leukemia. An important attribute of a white blood cell is the age of the cell; cells are grouped into discrete classes according to age. The numbers of cells in these age groups are important indicators. Automated counting techniques could save time and money. The traditional automatic approach to counting white blood cells is to segment, extract features, and classify the cells, respectively.[1,2] The traditional approach generally gives discrete counts but the counts are not truly discrete, since age is a continuous variable.

In this paper, we describe a novel approach that produces a count of the blood cells in each group but that does not rely on explicitly isolating and classifying the cells. A new algorithm based on morphological granulometries,[3–5,10–14] the granulometric mixing theorem,[6] and the mixture proportion estimation algorithm[7] is used to estimate the counts of six cell classes—myeloblast, promyelocyte, myelocyte, metamyelocyte, band, and PMN.

When a white blood cell becomes older, the nucleus changes shape and becomes smaller. Example gray scale images of all six cell classes of cell are depicted in Fig. 1 (ordered from youngest to oldest). Figure 1 also shows examples of hand-segmented nuclei. In this paper we assume that we have the segmented nuclei images as inputs. We are currently investigating the use of the full gray scale images.

Previously, the granulometric-mixing-theorem-based estimation algorithm was successfully used to estimate the counts and size information of standard geometric objects—rectangles, squares, circles, etc.—with an assumption of normal or gamma sizing distribution.[7] Nevertheless, direct application of the algorithm as suggested by Sand and Dougherty[7] is very difficult because convergence is rare; we could not achieve convergence to reasonable values for more than two classes of cells.[15] This is the motivation for the new algorithm, which does converge for the six cell classes that we have available.

The data used in the experiments are described in Sec. 2. Section 3 describes morphological granulometries, the granulometric mixing theorem, and the mixture proportion estimation algorithm. The new algorithm based on the granulometric mixing theorem is described in Sec. 4. The experimental description and the results are presented in Sec. 5. Section 6 concludes this paper.

2 Data Description

In the experiments we use bone marrow images collected at the University of Missouri Ellis-Fischel Cancer Center. Each white blood cell image is cropped and segmented

Paper 99011 received Mar. 23, 1999; revised manuscript received Dec. 8, 1999; accepted Feb. 23, 2000.
1017-9909/2000/$15.00 © 2000 SPIE and IS&T.

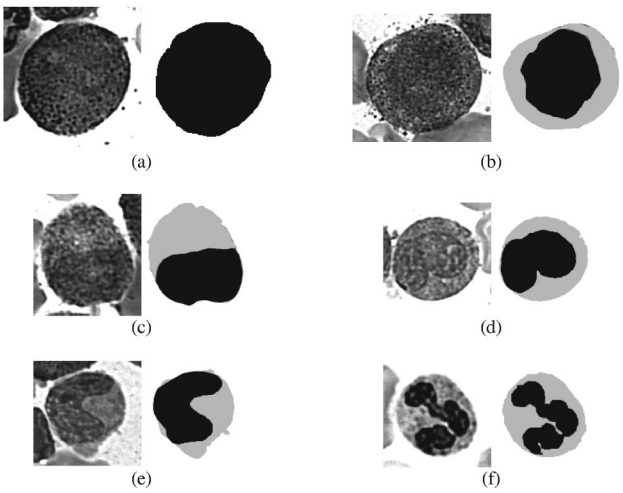

Fig. 1 Sample gray scale and corresponding hand-segmented images of white blood cell: (a) myeloblast, (b) promyelocyte, (c) myelocyte, (d) metamyelocyte, (e) band, and (f) PMN.

manually. The images were manually classified by Dr. C. William Caldwell, Professor of Pathology and Director of the Pathology Labs at the Ellis-Fischel Cancer Center. The data set consists of six classes of white blood cells—myeloblast, promyelocyte, myelocyte, metamyelocyte, band, and PMN. There are 20, 9, 130, 138, 42, and 149 hand-segmented images for all six classes of cells, respectively. Each hand-segmented image is composed of three regions—nucleus, cytoplasm, and background—with gray level $=0$, 176, and 255, respectively.

3 Morphological Granulometries

3.1 *Morphological Operations*

Morphological operations are nonlinear, translation invariant transformations. An excellent tutorial is given by Dougherty.[3] In this paper, we describe binary morphological operations only. Binary images can be considered as functions on arrays with values of 0 or 1 or, equivalently, as characteristic functions of subsets of the two-dimensional plane. The concept of structuring element is fundamental in morphology; it is the analogue of a convolution mask in linear image processing. A structuring element can be thought of as a small image, such as a 3×3 square. The basic morphological operations involving an image S and a structuring element E are

erosion: $(S\ominus E)(x)=\cap\{S-e:e\in E\}$,

dilation: $(S\oplus E)(x)=\cup\{E+s:s\in S\}$,

where $\cap$ and $\cup$ denote the set intersections and union, respectively. $A+x$ denotes the translation of a set A by a point x, i.e.,

$$A+x=\{a+x:a\in A\}.$$

The opening operation, derived from the erosion and dilation, is defined by

$$S\bigcirc E=(S\ominus E)\oplus E.$$

3.2 *Pattern Spectrum*

Pattern spectra are well described elsewhere.[3–5] Let E be a convex structuring element. Let $\Omega(t)$ be area of $S\bigcirc tE$ where t is a real number and $\Omega(0)$ is the area of S. $\Omega(t)$ is called a size distribution. The normalized size distribution $\Phi(t)=1-\Omega(t)/\Omega(0)$, and $d\Phi(t)/dt$ are called granulometric size distribution or pattern spectrum of S. The opening required for computing granulometries can be computed very efficiently using the opening transform developed by Chen and Haralick.[8]

3.3 *Granulometric Mixing Theorem*

Let S be a random set composed of randomly sized, disjoint translates arising from m compact sets $A_1, A_2, \ldots, A_m$, namely

$$S=\bigcup_{i=1}^{m}\bigcup_{j=1}^{n_i}(r_{ij}A_j+x_{ij}).$$

For the granulometry $\{S\bigcirc tE\}$ generated by a convex, compact set E, the kth pattern-spectrum moment of S is

$$\mu^{(k)}(S)=\frac{\sum_{i=1}^{m}\sum_{j=1}^{n_i}m[A_i]\mu^{(k)}(A_i)r_{ij}^{k+2}}{\sum_{i=1}^{m}\sum_{j=1}^{n_i}m[A_i]r_{ij}^{2}},$$

where $m[A_i]$ is the area of A_i and $\mu^{(k)}(A_i)$ is the kth pattern-spectrum moment of A_i.

For each i, $\mathbf{r_i}$ is a random variable. The scaling parameters r_{ij}, $j=1,\ldots,n_i$, are realizations of the random variable $\mathbf{r}_i$. The distributions of the random variables are called sizing distributions. Sand and Dougherty applied the granulometric mixing theorem[4] to problems involving normal and gamma sizing distributions using the method of moments.[7] The method assumes that the total number of the objects in the image is known. For each primitive class, a mean, variance, and proportionality constant must be found. A system of nonlinear equations needs to be solved to find those parameters. Thus, for example, 6, 9, and 18 unknowns need to be found for the two-class, three-class, and six-class problems, respectively. Furthermore, the equations involve powers of the unknowns that increase as the number of classes increases. For example, the three-class problem involves up to an eighth order equation. It is very difficult to achieve convergence when trying to solve these high order systems of nonlinear equations. The algorithm was applied to synthetic random images of standard geometric objects with normal and gamma size distributions.

4 Modified Mixture Proportion Estimation Algorithm

The modified algorithm is based on the granulometric mixing theorem. For this particular problem, we use prior information concerning the pattern spectra of the training samples for each class of cell to perform an initial segmentation of the pattern spectrum of a testing image containing an unknown number of cells. The initial segmentation is

used to reduce the problem of estimating the percentage of each type of primitive to that of estimating the number of occurrences of only one primitive, one problem for each cell class. Once these one primitive problems are solved, then the solutions are again refined using prior information. This reduction to a one primitive problem solves the convergence problem.

The modified algorithm uses the prior pattern spectra moments of cells to reduce the problem to a one-class problem, and considers only one class at a time. More specifically, the mean and variance of the training pattern spectra means are used in an optimal thresholding algorithm to identify potential locations at which to segment a testing pattern spectrum into individual components corresponding to single primitives.

If we assume that a portion of a pattern spectrum is produced by only one primitive, then the mixing theorem becomes

$$\mu^{(k)}(S)=\frac{\Sigma_{j=1}^{n}\mu^{(k)}(A)r_j^{k+2}}{\Sigma_{j=1}^{n}r_j^2},$$

using the method-of-moments yield

$$\mu^{(k)}(S)\mu^{(2)}=\mu^{(k)}(A)\mu^{(k+2)}, \tag{1}$$

where $\mu^{(k)}$ is the kth moment of the sizing distribution. In particular, if there is a single primitive and the sizing distribution is assumed normal, we use the following expressions:

$$\begin{aligned}\mu^{(2)}&=\mu^2+\sigma^2,\\ \mu^{(3)}&=\mu^3+3\mu\sigma^2,\\ \mu^{(4)}&=\mu^4+6\mu^2\sigma^2+3\sigma^4\end{aligned} \tag{2}$$

in Eq. (1) to yield the system of two equations and two unknowns

$$\begin{aligned}\mu^{(1)}(S)(\mu^2+\sigma^2)&=\mu^{(1)}(A)(\mu^3+3\mu\sigma^2),\\ \mu^{(2)}(S)(\mu^2+\sigma^2)&=\mu^{(2)}(A)(\mu^4+6\mu^2\sigma^2+3\sigma^4).\end{aligned} \tag{3}$$

The quantities $\mu^{(1)}(S)$, $\mu^{(2)}(S)$, $\mu^{(1)}(A)$, and $\mu^{(2)}(A)$ are known; the first two can be computed directly from the pattern spectrum of an input image and the latter two can be computed from a given primitive in a training set. These equations are solved numerically for each member of some set of the primitives in the training set. Each solution produces an estimate of the total number of cells in the corresponding class. These estimates are averaged to produce a final estimate of the number of cells in the corresponding class.

We can estimate the number of objects produced by a particular primitive assuming all objects are produced by only that primitive. Assume n objects are produced by primitive A. Each object is of the form r_jA where r_j is a scaling factor, $j=1,\ldots,n$. We calculate the total area, $m[S]$, by

0	1	1	0
1	1	1	1
1	1	1	1
0	1	1	0

Fig. 2 The structuring element used in the experiments.

$$m[S]=\sum_{j=1}^{n} m[A]r_j^2.$$

Using the sample moment yields

$$m[S]=nm[A]\mu^{(2)}.$$

The normal sizing distribution assumption yields

$$m[S]=nm[A](\mu^2+\sigma^2).$$

Therefore the total number of objects, n, can be estimated by

$$n=\frac{m[S]}{m[A](\mu^2+\sigma^2)}. \tag{4}$$

In the experiments we use the structuring element shown in Fig. 2 because it yields pattern spectra of cell images that have small left tails. Figure 3 displays samples of pattern spectra of all six classes of cells corresponding to this structuring element.

4.1 *Algorithm Description*

The algorithm consists of two phases: a training phase and a testing, or operational, phase. The training phase consists of computing prior information that is used in the operational phase. In the operational phase, the single class proportion estimation algorithm (SPEA) is applied to an image containing an unknown number of cells of each type and produces an estimated count using the prior information, the one-primitive version of the mixing theorem, and some refinements.

The basic idea in the operational phase in the SPEA is to use prior information to initially segment the pattern spectrum into six components, one for each cell class. The one-primitive version of the mixing theorem is applied to each component separately several times, one for each primitive in a subset of the training images. The Newton–Raphson iterative algorithm for solving nonlinear systems of equations is applied to Eq. (3). It does not always converge. Each time that it does converge, a count is generated. These counts are average to produce the final estimate. These steps are made specific in steps 3.7 and 3.8 of the operational phase algorithm. There is also some processing to factor out the effects of overlapping distributions of the pattern spectra. The average of the left tails of younger cells is scaled, and subtracted from the pattern spectrum in the current stage before the estimation of the next older cell is applied.

The application of one-primitive version of the mixing theorem allows the algorithm to use more than one primi-

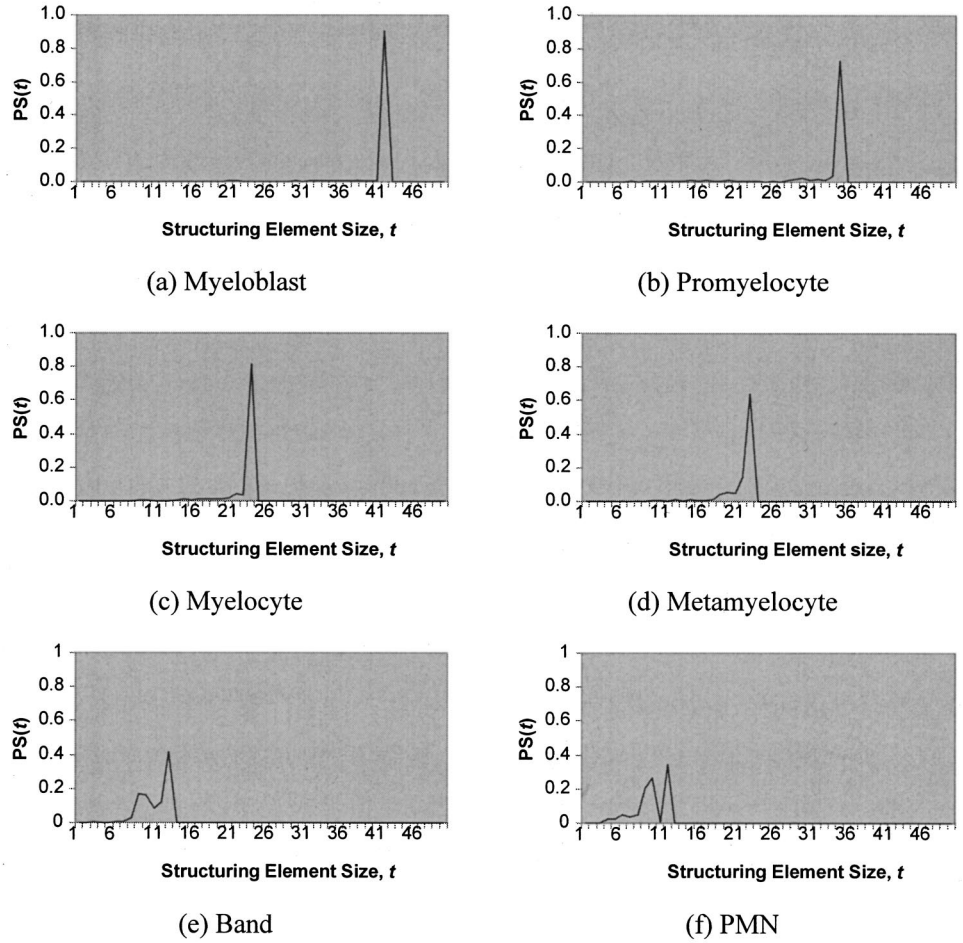

Fig. 3 Sample pattern spectra of all six cell classes corresponding to structuring element in Fig. 2.

tive from each class. This is an advantage of the algorithm because in a cell image, unlike an image containing standard geometric shaped objects, there are variations of shapes of cell, even from the same class. In other words, the primitive themselves are random sets. A single primitive cannot represent a cell class well.

To initially segment a pattern spectrum into components, initial segmentation points (ISPs) are found. Consider, for example, the particular samples of myeloblast and promyelocyte in Fig. 3. From those particular samples, we can see that choosing an ISP of about 38 would separate the two pattern spectra quite well. That is, if the input image consisted only of the two cells that produced the pattern spectra shown in Figs. 3(a) and 3(b), then the pattern spectrum of the input image would be the sum of those two pattern spectra. The information above structuring element size 38 is produced only by the myeloblast and below 38 only by the promyelocyte. Thus, we could apply the one-primitive mixing theorem to each component to estimate the number of cells of each type that are present. This idea works well when the left tail of the pattern spectrum produced by each primitive is small and the pattern spectra of cells from each class are well separated.

Of course, a real input image would have contributions from many cells of each type so the separation of the pattern spectra is not so clear. Therefore, we use optimal thresholding and refinement. The algorithm for the six-class problem is described below.

Training Phase

1. Calculate the pattern spectra of all training images.
2. Calculate the mean of each pattern spectrum, PSM_{ij}, for $i=1,2,\ldots,6$ and $j=1,2,\ldots,m_i$ where m_i = number of training samples from class i.
3. For each cell class, compute the mean and variance of PSM_{ij}, $\mu_i=\mathrm{mean}(\mathrm{PSM}_{ij})$ and $\sigma_i^2=\mathrm{variance}(\mathrm{PSM}_{ij})$, $i=1,2,\ldots,6$.
4. Calculate ISPs: Use the obtained means and variances to calculate the initial thresholds by solving the following equation[9] for each pair of adjacent classes:
$$AT^2+BT+C=0, \quad (5)$$
where
$A=\sigma_i^2+\sigma_{i-1}^2$, $B=2(\mu_i\sigma_{i-1}^2+\mu_{i-1}\sigma_i^2)$,
$C=\mu_{i-1}^2\sigma_i^2-\mu_i^2\sigma_{i-1}^2+2\sigma_i^2\sigma_{i-1}^2\ln(\sigma_{i-1}P_i/\sigma_iP_{i-1})$,
$i=2,\ldots,6$.
In the experiment we assume that the prior probabilities are all equal, i.e., $P_i=P_{i-1}$.

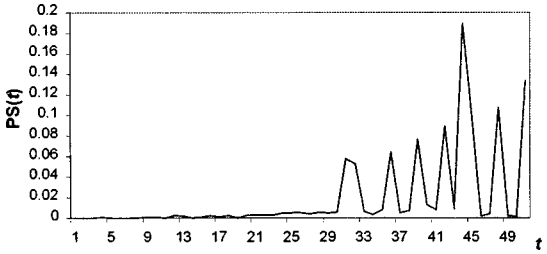

Fig. 4 Pattern spectrum of an image containing 10 myeloblasts.

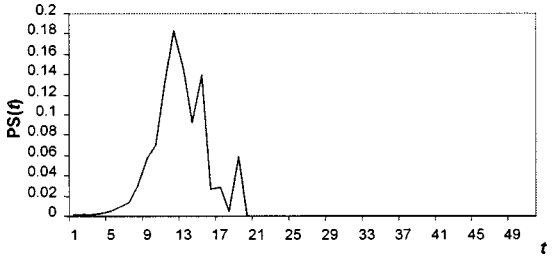

Fig. 6 Pattern spectrum of an image containing 20 bands.

5. Select ten samples from each class to be used in the averaging process in the operational phase.

Operational Phase

1. Compute the un-normalized pattern spectrum, PS of the input image S.
2. Find segmentation points as follows: For each ISP_i, find the point that has the minimum value of PS in a 4×1 window around the ISP: PS(ISP-1) to PS(ISP $+2$). Call the ith one T_i, $i=2,3,\ldots,6$. Let T_1 $=\mathrm{length(PS)}+1$, and $T_7=1$, and note that T_i $>T_{i+1}$.
3. Estimate the number of cells in each class:
   For $i=2$ to 7
   Set nprims$=0$.
   For $j=1$ to 10
   3.1 Let A_{ij} be the jth primitive from class i.
   3.2 Let PA_{ij} be the un-normalized pattern spectrum of A_{ij}.
   3.3 Set $\mathrm{tail}(\mathrm{PA}_{ij})=\mathrm{PA}_{ij}(t)$, for $t=1,\ldots,T_i-1$.
   3.4 Set $\mathrm{PA}_{ij}(t)=0$, for $t=1,\ldots,T_i-1$.
   3.5 Set $\mathrm{PS}_i(t)=\mathrm{PS}(t)$, for $t=T_i,\ldots,T_{i-1}-1$.
   3.6 Set $\mathrm{PS}_i(t)=0$, for $t=1,\ldots,T_i-1$.
   3.7 Estimate μ and σ for the one-primitive problem, where the input pattern spectrum is PS_i, and the pattern spectrum of the primitive is PA_{ij}, using the Newton–Raphson algorithm to solve the system of Eqs. (3).
   3.8 If the algorithm converges, then
   Set nprims$=$nprims$+1$.
   Estimate the count of class i from the jth primitive, $n_{i,\mathrm{nprims}}$ by

$$n_{i,\mathrm{nprims}}=\frac{\sum_{t=T_i}^{T_{i-1}-1}\mathrm{PS}_i(t)}{(\mu^2+\sigma^2)\sum_{t=T_i}^{\mathrm{length(PA}_{ij})}\mathrm{PA}_{ij}(t)}.$$

   Estimate the tail produced by the primitive from class i by
   $\mathrm{PA}_{i,\mathrm{nprims}}=\mathrm{tail}(\mathrm{PA}_{ij})$.
   End (For $j=1$ to 10).
   Average n_{ij}, $j=1,2,\ldots,$nprims, to get an estimated count of class i, $\overline{n_i}$, by

$$\overline{n_i}=\frac{\sum_{j=1}^{\mathrm{nprims}}n_{ij}}{\mathrm{nprims}}.$$

   Average PA_{ij}, $j=1,2,\ldots,$nprims, to get an estimated tail of class i, $\overline{\mathrm{PA}_i}$, by

$$\overline{\mathrm{PA}_i}=\frac{\sum_{j=1}^{\mathrm{nprims}}\mathrm{PA}_{ij}}{\mathrm{nprims}}.$$

   Subtract the scaled tail from PS to get rid of the effect of the left tail from the current primitives pattern spectrum on the pattern spectra of the smaller primitives by subtracting $\overline{n_i}$, $\overline{\mathrm{PA}_i}$ from $\mathrm{PS}(t)$, t $=1,\ldots,T_i-1$.
   End (For $i=2$ to 7).

It should be noted that $\mathrm{PS}(t)$ and $\mathrm{PA}_{ij}(t)$ are the un-normalized versions of the pattern spectra, i.e., $\Phi(t)$ $=\Omega(0)-\Omega(t)$ (see Sec. 3.2). In other words, they are the scaled versions of the pattern spectra with the areas of S and A_{ij} as the scaling factors, respectively. The summations over the whole t axis of $\mathrm{PS}(t)$ and $\mathrm{PA}_{ij}(t)$ yield the areas of S and A_{ij}, successively.

Figures 4, 5, and 6 show pattern spectra of images containing 10 myeloblasts, 10 myelocytes, and 20 bands, respectively. Figure 7 depicts a pattern spectrum of an image consisting of 10 myeloblasts, 10 myelocytes, and 20 bands that is a combination of the previous three figures. In this case we have ISPs$=30$ and 15, and $T_1=52$, $T_2=30$, and $T_3=18$. From the three figures that show the pattern spec-

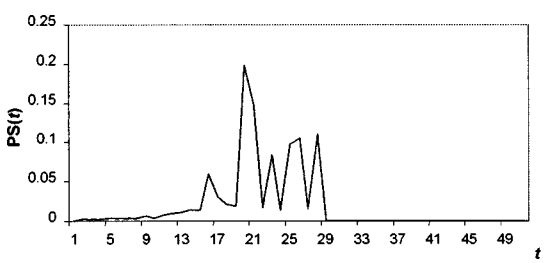

Fig. 5 Pattern spectrum of an image containing 10 myelocytes.

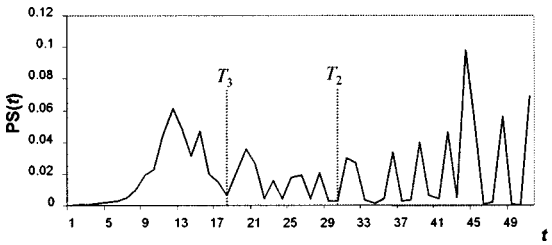

Fig. 7 Pattern spectrum of the three-class image displayed in Fig. 10, $T_1=52$, $T_2=30$, and $T_3=18$ for this pattern spectrum.

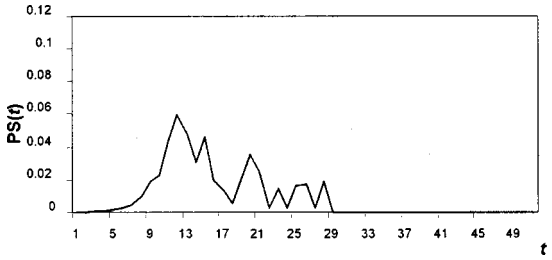

Fig. 8 Remaining pattern spectrum after the subtraction of the left tail of myeloblasts.

trum of each type of cell individually, the derived segmentation points are very reasonable. In the first step only the segment of the pattern spectrum in which t ranges from 30 to 51 is considered to be a segment produced by the myeloblasts. The estimated number of myeloblasts is 9.73. This number is used as a scaling factor to subtract the left tail of myeloblast from the input pattern spectrum.

Figure 8 shows the remaining pattern spectrum after the number of myeloblasts is estimated. The pattern spectra before and after the subtraction of the tail of myeloblasts are very similar, especially when $t<20$. It is not obvious to notice the difference in the pattern spectrum plots. The values of the pattern spectra, $t=20$ to 29, are provided in Table 1. The pattern spectrum values in Table 1 show how small the left tails of myeloblasts are. After eliminating the effect of myeloblasts, it is assumed that the remaining pattern spectrum in Fig. 8 represents the pattern spectrum produced by myelocytes and bands only. A similar process is performed to this remaining pattern spectrum to estimate the number of myelocytes ($t=18$ to 29). After eliminating the effect of myelocytes, the final remaining segment is assumed to be produced by bands.

5 Experimental Description and Results

We separated the data set into training and testing sets by randomly selecting 10, 9, 40, 15, 12, and 45 images of myeloblast, promyelocyte, myelocyte, metamyelocyte, band, and PMN, respectively, to be the testing set. The remaining images are in the training set. The training set consists of 10, 9, 90, 23, 30, and 104 images of the six classes of cells, respectively. We make a note that because only 9 images of the promyelocyte class are available, we use them as both training and testing sets.

The testing images are created by randomly selecting the cells from the testing set and putting them into images. We created three testing images for two-class, three-class, and six-class problems. The two-class image consists of 10 myeloblasts and 20 bands. The three-class image consists of

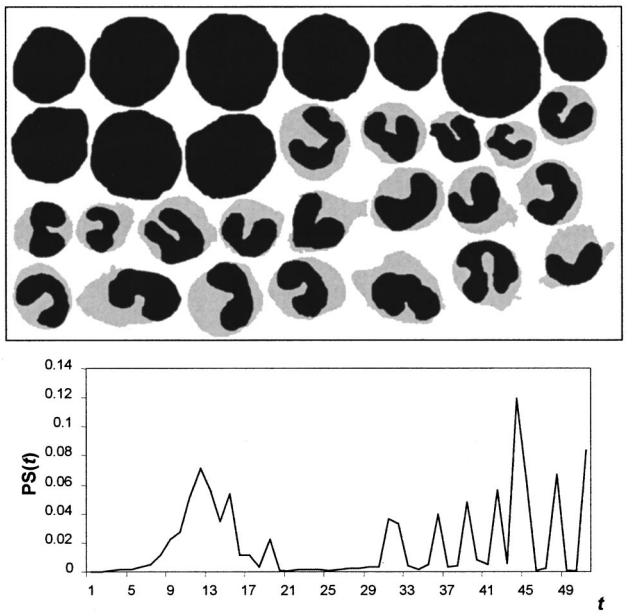

Fig. 9 Testing image (532×992) with 10 myeloblasts and 20 bands, and its corresponding pattern spectrum.

10 myeloblasts, 10 myelocytes, and 20 bands. The six-class image consists of 10 myeloblasts, 9 promyelocytes, 21 myelocytes, 10 metamyelocytes, 12 bands, and 20 PMNs. These three testing images and their corresponding pattern spectra are shown in Figs. 9–11.

5.1 *Results From the Granulometric Mixing Theorem*

Assuming that the sizing distribution of cell is normal, we need to solve for the number of cells (n), the mean (μ), and standard deviation (σ) of each class. In the two-class image we initialize $[n_1,n_2,\mu_1,\mu_2,\sigma_1,\sigma_2]=[15,15,1.2,1.2,0.1,0.1]$. we also need to set the total number of cells to the actual number, 30. The algorithm converges to [11.14, 18.86, 1.33, 1.10, 0.15, 0.30]. The estimated counts, 11.14 and 18.86, are close to the human expert's numbers, 10 and 20. Nevertheless, for the three-class and six-class images, with a variety of initializations, the algorithm does not converge correctly. Some n_i converge to zero, and some μ_i and σ_i converge to very large numbers.

Table 1 Some values of the remaining pattern spectrum, $t=20$ to 29, before and after the subtraction of the left tail of myeloblasts.

t	20	21	22	23	24	25	26	27	28	29
PS(t) Before	0.036	0.026	0.004	0.016	0.004	0.018	0.020	0.004	0.021	0.003
PS(t) After	0.035	0.026	0.003	0.015	0.002	0.016	0.017	0.003	0.019	0.000

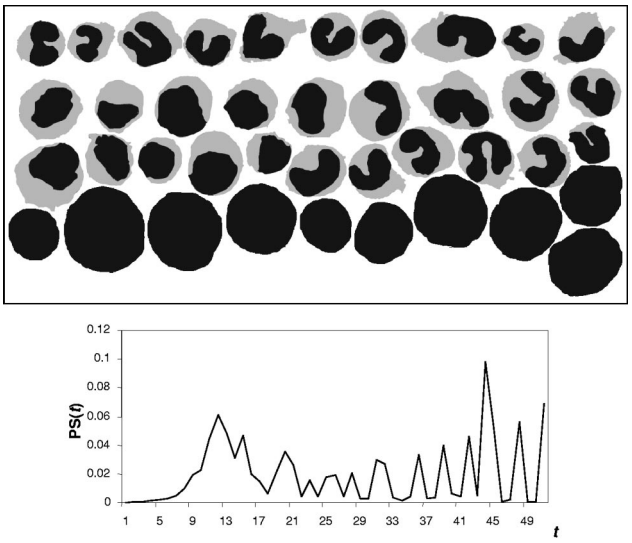

Fig. 10 Testing image (586×1240) with 10 myeloblasts, 10 myelocytes, and 20 bands, and its corresponding pattern spectrum.

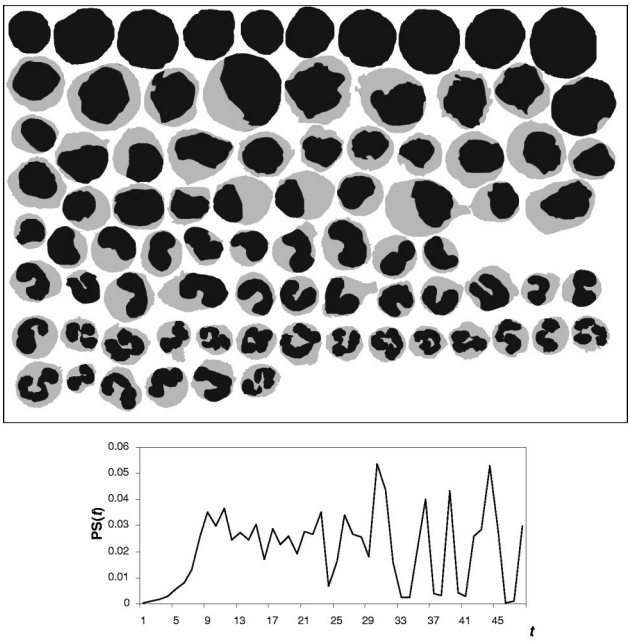

Fig. 11 Testing image (1000×1500) with 10 myeloblasts, 9 promyelocytes, 21 myelocytes, 10 metamyelocytes, 12 bands, and 20 PMNs, and its corresponding pattern spectrum.

5.2 *Results From the Modified Algorithm*

The means and variances of the means of pattern spectrum of all six classes of cell calculated from the training set are shown in Table 2.

From Table 2, for the six-class problem, solving Eq. (4) yields the ISPs of 36, 27, 21, 16, and 11 for $i=2-6$, respectively. The segmentation points of 38, 29, 20, 16, and 12 are then found using these ISPs. For the two-class problem, the ISP is 20, the segmentation point is 21. The ISPs are 31 and 16, and the segmentation points are 30 and 18, in the three-class problem.

The results of the SPEA are shown in Table 3.

The result of the SPEA on the two-class image is close to the human expert's numbers because the pattern spectra are well separated. The three-class image produces a pattern spectrum that has no obvious segmentation points. Nonetheless, the algorithm yields the estimated numbers that are close to the human expert's ones. In the six-class problem, the numbers are reasonable. About one myeloblast is counted as promyelocyte, about three myelocytes are counted as about one promyelocyte and about two metamyelocytes. There are overestimated numbers of bands and PMNs. The results show that there are some miscounts in the adjacent classes. This is not surprising

Table 2 Means and variances of the means of pattern spectrum of all six classes of cell in the training set.

	Myeloblast	Promyelocyte	Myelocyte	Metamyelocyte	Band	PMN
Mean [Mean(PA)]	39.43	31.53	21.86	20.36	12.25	9.87
Var [Mean(PA)]	26.91	20.13	26.39	25.87	4.32	4.32

Table 3 Results of the SPEA on three testing images.

		Number of Cells						
		Myeloblast	Promyelocyte	Myelocyte	Metamyelocyte	Band	PMN	Total
Two-class image	Human expert	10	⋯	⋯	⋯	20	⋯	30
	Algorithm	9.64	⋯	⋯	⋯	19.52	⋯	29.16
Three-class image	Human expert	10	⋯	10	⋯	20	⋯	40
	Algorithm	9.73	⋯	9.13	⋯	19.21	⋯	38.07
Six-class image	Human expert	10	9	21	10	12	20	82
	Algorithm	9.01	10.76	18.24	11.87	15.99	21.24	87.11

because the nucleus of the adjacent classes has very similar sizes and shapes. Let the percentage error be $\Sigma_{i=1}^{m}|n_i - \overline{n_i}|/\Sigma_{i=1}^{m} n_i \times 100\%$, where m is the number of classes, n_i and $\overline{n_i}$ are the human expert's and estimated numbers of cells in class i, respectively. The errors for two-class, three-class, and six-class problems are 2.80%, 5.72%, and 15.38%, respectively. In all three cases, the estimated total numbers of cells in the results are close to the actual total numbers of cells. The errors of the estimated total numbers of cells, $|\Sigma_{i=1}^{m} n_i - \Sigma_{i=1}^{m} \overline{n_i}|/\Sigma_{i=1}^{m} n_i \times 100\%$, are 2.8%, 4.8%, and 6.2%, for the two-class, three-class, and six-class problems, respectively.

6 Conclusion

The modified algorithm yields good results for the white blood cell counting problem. A key aspect of the method is that we use prior statistics concerning the pattern spectra of each class of cell to ease the convergence problem by reducing the multi-class problem to several single class problems. The averaging in the count estimate and the tail subtraction allow more than one primitive from each class to be applied to the modified algorithm. Therefore the cells do not need to be produced by any particular primitives. In the future, we intend to investigate the use of random sets as models of shape primitives.

Other possible applications of this method include mixture estimation for silver-halide photographic *T*-grain crystals,[7] highway concrete inspection systems, fish counting, and other areas for which we need to count the number of shapes of different types in an image, but for which the shapes are difficult to segment.

References

1. J. Park and J. Keller, ''Fuzzy patch label relaxation in bone marrow cell segmentation,'' *IEEE Int'l Conference on Systems, Man, and Cybernetics*, pp. 1133–1138, Orlando, FL, October (1997).
2. M. Beksaç, M. S. Beksaç, V. B. Tipi, H. A. Duru, M. U. Karakas, and A. Nur Çakar, ''An artificial intelligent diagnostic system on differential recognition of hematopoietic cells from microscope images,'' *Cytometry* **30**, 145–150 (1997).
3. E. R. Dougherty, *An Introduction to Morphological Image Processing*, SPIE, Bellingham, WA (1992).
4. E. R. Dougherty and F. Sand, ''Representation of linear granulometric moments for deterministic and random binary Euclidean images,'' *J. Visual Commun. Image Represent* **6**(1), 69–79 (1995).
5. P. Maragos, ''Pattern spectrum and multiscale shape representation,'' *IEEE Trans. Pattern Anal. Mach. Intell.* **11**(7), 701–716 (1989).
6. F. Sand and E. R. Dougherty, ''Asymptotic normality of the morphological pattern-spectrum moments and orthogonal granulometric generators,'' *J. Visual Commun. Image Represent* **3**(2), 203–214 (1992).
7. F. Sand and E. R. Dougherty, ''Asymptotic granulometric mixing theorem: Morphological estimation of sizing parameters and mixture proportions,'' *Pattern Recogn.* **31**(1), 53–61 (1998).
8. S. Chen and R. M. Haralick, ''Recursive erosion, dilation, opening and closing transforms,'' *IEEE Trans. Image Process.* **4**(3), 335–345 (1995).
9. R. C. Gonzalez and R. E. Woods, *Digital Image Processing*, Addison–Wesley, New York (1993).
10. E. R. Dougherty, *Random Processes for Image and Signal Processing*, SPIE, Bellingham, WA, and IEEE, New York (1999).
11. E. R. Dougherty, J. B. Pelz, F. Sand, and A. Lent, ''Morphological image segmentation by local granulometric size distributions,'' *J. Electron. Imaging* **1**(1), 46–60 (1992).
12. R. M. Haralick and L. G. Shapiro, *Computer and Robot Vision*, Addison–Wesley, New York (1992).
13. G. Matheron, *Random Sets and Integral Geometry*, Wiley, New York (1975).
14. J. Serra, *Image Analysis and Mathematical Morphology*, Academic, New York (1983).
15. N. Theera-Umpon and P. D. Gader, ''Automated white blood cell counting via classification-free granulometry methods,'' *Nonlinear Image Processing X, Proc. SPIE* **3646**, 260–269, Jan. (1999).

Nipon Theera-Umpon has been working toward Ph.D. degree in Electrical Engineering at the University of Missouri-Columbia since 1996. He received the B.Eng (Hons.) degree from Chiang Mai University, Thailand, and the M.S. degree from the University of Southern California, both in Electrical Engineering, in 1993 and 1996, respectively. From March 1993 to December 1994, he worked at the Department of Electrical Engineering, Chiang Mai University, where he is currently a leave-of-study faculty member. He received a full scholarship from the Royal Thai Government to pursue a Master's and Ph.D. degrees in the U.S. in December 1994. His research interests include mathematical morphology, random processes, neural networks, communication systems, and signal and image processing.

Paul Gader received his Ph.D. from the University of Florida in 1986. After receiving his Ph.D. for research in image processing, he worked as a Senior Research Scientist at Honeywell Systems and Research Center, as an Assistant Professor of Mathematics at the University of Wisconsin–Oshkosh, and as a Research Engineer and Manager at the Environmental Research Institute of Michigan (ERIM). He is currently an Associate Professor in the department of Computer Engineering and Computer Science at the University of Missouri–Columbia. Dr. Gader has worked on a wide variety of basic and applied research problems, including mathematical morphology in image processing, medical imaging, landmine and unexploded ordnance detection, handwriting recognition and document analysis systems, automatic target recognition, and object recognition, fuzzy sets in computer vision, medical imaging, and applied mathematics.